

Model for multimode picosecond dynamic laser chirp based on transmission line laser model

A.J. Lowery

Indexing terms: Lasers, Transmission lines, Semiconductor lasers

Abstract: Laser chirp contributes significantly to the linewidth of near single-mode injection modulated semiconductor laser devices, and is a consequence of the carrier dependence of the active layer's refractive index. A model is developed that can accurately predict the multimode chirped spectra of Fabry-Perot devices based on the transmission line laser model (TLLM), with the addition of a transmission line stub and attenuator to the end facets. This time-domain model is easily interfaced to both drive circuit and fibre impulse response models. A 1550 nm InGaAsP device model under picosecond modulation is tested against experimental and analytical results of other workers.

1 Introduction

A knowledge of the spectral output of semiconductor lasers under pulse modulation is essential for the design of devices for high-data-rate long-haul fibre-optic transmission systems [1, 2, 3]. Such devices are usually single-mode to minimise fibre dispersion. However, this is considerably increased by the phenomenon of dynamic linewidth broadening [4, 5, 6, 7, 8], a.k.a. laser chirp. It is desirable, therefore, to be able to model the device to optimise its parameters for minimum linewidth before the fabrication stage is reached. The ideal model should be computationally efficient, accurate, easy to understand, and simple to modify to cope with future developments [9]. It should also be designed to link into larger system models, by the provision of suitable interfaces. The paper presents such a model, developed from an earlier model by the author [10], which has been specifically designed for multimode and single-mode devices where laser chirp is a significant factor. Its interfaces are a sampled drive current waveform and an optical output waveform, which allow for easy connection to drive circuit and fibre impulse response models.

The transmission line laser model (TLLM) was developed to investigate the spectra of multimode lasers under modulation. It is based on the transmission line modelling (TLM) method for fields [11, 12], and uses series connected transmission lines to model the longitudinal variation of optical electrical field in the lasing cavity. The wavelength dependence of the material gain is represented by the response of transmission line filters,

whose parameters are governed by the local carrier concentration. Unlike other multimode models, which provide the power envelope of the laser output for each discrete mode [13, 14, 15], the TLLM provides a sampled optical output waveform. A Fourier transform may then be used to convert the waveform into a continuous spectrum over a given bandwidth. Alternatively, the sample waveform may be convolved with the impulse response of the transmission fibre. This gives the pulse shape at the photodetector end of the fibre, and will show accurately the magnitude of the spectral dispersion along the fibre. In general, the optical output may be directed to any other transmission line model, such as those for semiconductor laser amplifiers, photodiodes or filters. This feature is one of the principle advantages of adopting transmission line modelling for optical systems. The model has proved to be faster than a standard numerical solution to the multimode rate equations when a longitudinal gain dependence is required.

Although the above model is useful in obtaining an estimate of the spectral width of multimode lasers, it neglects laser chirping, an important factor in the determination of the linewidth of modulated single mode lasers. This effect, which results from the carrier concentration dependent refractive index [16, 17, 18], is also fundamental in the study of bistability in laser amplifiers [19] and in multi-cavity devices [20].

Other models are available to estimate the chirp under large-signal modulation. These fall into two categories, (a) analytical and (b) numerical. The former rely on simplifying approximations, usually that the optical pulse envelope has a Gaussian form, and the carrier concentration falls linearly during this pulse [7, 8, 21]. This yields the expression

$$t_{1/2} f_{1/2} = 0.44\sqrt{1 + \alpha^2} \quad (1)$$

where

$t_{1/2}$ is the FWHM of the optical pulse,

$f_{1/2}$ is the FWHM of the spectrum,

α is the linewidth enhancement factor [17].

Although the above will be shown to give an accurate estimate of the spectral width, the predicted form of the spectrum is completely different, being a Gaussian shape rather than the commonly observed 'rabbit ear' shape [22, 23, 24, 25]. A more complete analysis [26] does however include the effects of pulse shape. Another analytical approximation used to calculate the pulse dispersion in single-mode fibres [6, 27] assumes that the laser is blue-shifted for half a relaxation oscillation period at the onset of a bit-period pulse, and is similarly red-shifted at the pulse end. This treatment effectively divides the power spectrum into three: red-shifted, blue-shifted and not-shifted. This may be satisfactory for long pulses, but

Paper 5793J (E13/E3), first received 1st July 1987 and in revised form 13th October 1987

The author is with the Department of Electronic and Electrical Engineering, Nottingham University NG7 2RD, United Kingdom

will become inaccurate as the pulse length is reduced below the relaxation period.

Numerical models of chirp are commonly based on a rate equation analysis of photon and carrier densities. Simple models give the instantaneous frequency by direct relation to the carrier density waveform [28]. Andersson and Andersson [29] use a Fourier transform of the instantaneous phase and power given by a numerical solution of the above equations, to produce the power spectral density (psd) for a single longitudinal mode. Similarly, Abdula and Saleh [30] use a Wigner distribution function to represent the spectra from a random noise driven single-mode numerical solution of the rate equations. Osinski & Adams [31, 32] obtain the psd of a multi-mode device without using a Fourier, or other, transform. This is achieved by splitting the optical pulse into time segments and then allocating the power of each segment to an appropriate frequency 'channel' depending on the presiding carrier concentration. This model produces an unrealistic spectral resolution, i.e. very narrow ears. This problem is resolved by Bickers and Westbrook [33] who convolve the spectrum with the response of the measuring equipment to find the observable spectrum.

The paper is partitioned in the following manner: Section 2 investigates possible methods of including chirp in the TLLM, and hence justifies the use of a 'stub-attenuator' model. Section 3 deals with the theory of the stub-attenuator model, its implementation, and the accuracy of mode position. Section 4 investigates the chirp of a pulse-modulated multi-mode 1.55 μm laser. The spectra of the laser are compared with both experimental data and the analytical model given by eqn. 1. Section 6 draws this paper to a conclusion, and suggests future areas of application of the TLLM.

2 Choice of model

The effect of laser chirp is to shift the output wavelength of all the modes of the resonant laser cavity. This is because a change in carrier concentration will modulate the refractive index of the active region which, in turn, produces a smaller modulation of the effective index, n_e , of the waveguide [34]. The latter governs the phase length of the Fabry-Perot resonant cavity, so shifting the cavity's resonant modes. This section reviews the choices available to achieve a suitable model of the above, by modification of Reference 10. It is not intended to discuss the causes and effects of the carrier dependence, a detailed review of which can be found in [17].

One obvious model stems from the Kramers-Kronig relationship, linking the refractive index shift to the wavelength dependence of material gain. The TLLM uses filters to represent the gain curve's frequency dependence. These also introduce a phase shift, also governed by the same relationship. Thus, if the filters accurately model the gain curve of the material, then the refractive index variation would also be modelled. However, owing to the asymmetry of the gain curve, and its sharp frequency dependence, an accurate model is difficult to achieve, and such a model would impose heavy penalties on computational time. Therefore the Lorentzian model of the gain curve introduced in [10] has been retained. This uses a second order bandpass filter based on transmission line stub components. Because of its symmetrical nature, this has zero phase-shift at the laser resonance, and so some other method of obtaining the required phase shift must be found.

A technique designed to extend TLM to model inhomogeneous waveguides [12] was then investigated. This uses open circuit transmission line stubs to capacitively load the transmission lines representing the cavity, thus reducing the phase velocity along the lines. In the TLLM, a stub was used at every node, its impedance, and hence capacitance being dependent upon the local carrier concentration. However this produced an unstable model which oscillated at half the Nyquist sampling frequency. This problem was caused by the introduction of gain between the loading stubs, which reflect part of the incident wave according to their impedance. These tend to split the main cavity into resonant subsections, each with gain. Power circulates and is amplified in these resonators, until the model becomes unstable. Several techniques were tried to solve this problem, including attenuation of the backward wave and the stored energy in the stub, however none proved successful.

The shift in the cavity resonance could be modelled by altering the cavity length to simulate a shift in effective index. For example, an increase in effective index by Δn_e over a value of n_e can be simulated by an increase in cavity length l over the normal value L . This approach neglects any effects of inhomogeneous effective index, such as intra-cavity reflections at impedance boundaries. However, as the index modulation along the cavity is slowly varying, in terms of wavelengths, and is in any case small, then these effects will also be small. The use of a multilongitudinal-section model is still justified as inhomogeneous carrier distribution will shift local gain curve spectra, leading to a wider effective gain bandwidth and so more modes, particularly in low facet reflectivity devices. A difficulty imposed by transmission line modelling is that it uses lines of a fixed length. As the cavity is an integer number of sections long, this implies that the cavity length could only be increased in discrete steps. As the section lengths are kept as long as possible, to minimise computational time, this would give unacceptable inaccuracy in the frequency domain.

A solution to this problem is to represent a small section at the end of the cavity and the facet by an impedance, the value of which is given by standard transmission line equations for the input impedance of terminated lines. This may then be equated to the input impedance of a network modelled with transmission line stubs. Two possibilities exist:

(a) to model the imaginary component of the impedance with a transmission line stub, and the real component with a resistor: the 'stub-resistor' model

(b) to model the impedance with an attenuator matched to the reflectivity of the facet, and a stub to account for the phase shift of the cavity: the 'stub-attenuator' model

These are shown in Figs. 1a and 1b, respectively.

In both these models, the impedance is matched at one frequency only, usually the laser's resonance frequency. This introduces inaccuracy away from the resonance frequency. The TLM stub model also introduces inaccuracy, particularly if undersampling is used. However, studies show that both of these errors are insignificant, as the laser bandwidth is a small fraction of the model's bandwidth.

Both stub-resistor and stub-attenuator models of a cavity were investigated for frequency and phase response. The theory and results of these tests will be dealt with in the next section. However, the stub attenuator model showed a distinct, and intuitively obvious,

advantage, this being a 'flat' facet amplitude response. This contrasts with the stub-resistor model whose response is frequency dependent, and so causes a shift in

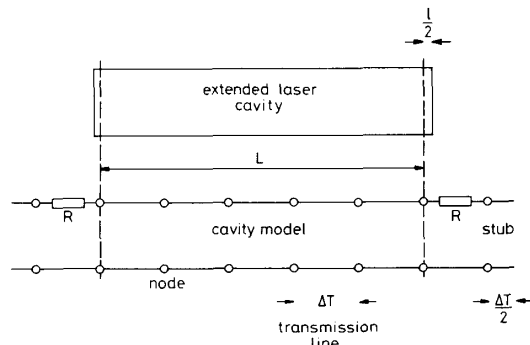


Fig. 1a Laser cavity and associated stub-resistor model

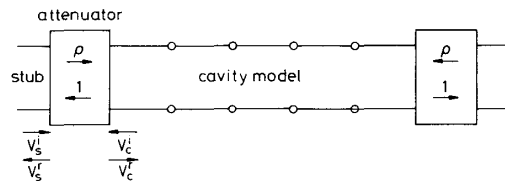


Fig. 1b Stub-attenuator model

the laser central resonance from the gain curve peak. For this reason the rest of the paper will concentrate on the stub-attenuator (SA) model.

3 Stub-attenuator theory

The basis for the SA model is that a short extension is added between the cavity and the laser facet, usually at each end of the cavity. The length of this being dependent on the required wavelength increase in the main cavity. The attenuating effect of the end facet is then moved from the end of the cavity extension to the end of the main cavity. This allows the electric field in the cavity extension to be modelled by the voltage on an open circuit transmission line stub. This technique gives a flat frequency response as the stub itself is lossless, and the attenuator has a flat frequency response.

The stub length is fixed at one half an iteration timestep, ΔT , long. This ensures that a sample pulse, reflected into the stub, arrives at the stub terminals for the next iteration. Its impedance is made variable to enable different cavity lengths to be accommodated. This impedance is found by equating the stub's input impedance to the input impedance of the cavity extension.

The former is given by

$$Z_{is} = Z_s / j \tan(\pi f \Delta T) \quad (2)$$

where

Z_s is the stub impedance
 f is the laser resonance frequency

The latter is given by

$$Z_{ic} = Z_c / j \tan(\beta l) \quad (3)$$

where

Z_c is the cavity wave impedance ([10], eqn. 3)
 l is the extra cavity length

β is the propagation constant inside the cavity

Thus

$$Z_s = Z_c \tan(\pi f \Delta T) / \tan(\beta l) \quad (4)$$

The above equation is valid when eqn. 2 is positive, i.e. the stub impedance is positive. When eqn. 2 is negative, then the input impedance of the cavity may be modelled using a short-circuited transmission line stub, and eqn. 3 becomes

$$Z_s = -Z_c / [\tan(\pi f \Delta T) \tan(\beta l)] \quad (5)$$

The stub and attenuator can now be represented by a scattering matrix, which describes the relation between reflected and incident pulses at the last cavity node. If ρ is the field reflectivity of the facet, then this matrix is

$$\begin{bmatrix} V_c^r \\ V_s^r \end{bmatrix} = \frac{1}{Z_s + Z_c} \begin{bmatrix} \rho(Z_s - Z_c) & 2\rho Z_c \\ 2Z_s & (Z_c - Z_s) \end{bmatrix} \begin{bmatrix} V_c^i \\ V_s^i \end{bmatrix} \quad (6)$$

where

V_c^i is the incident pulse from the cavity (see Fig. 1b)
 V_c^r is the reflected pulse into the cavity
 V_s^i is the incident pulse from the stub
 V_s^r is the reflected pulse into the stub

As the stub is one half of one iteration timestep long, a reflected pulse into it will become an incident pulse upon the scattering node one iteration later. For a short-circuited stub, the phase of the pulse will be reversed upon reflection at the end of the stub. The above matrix leads to a simple numerical routine in which the reflected pulses out of each node are calculated from the incident pulses, and vice-versa for each iteration.

The effect on absolute frequency of the central mode, and on modal spacing, of increasing the model's length by l , can be compared to the theoretical result to obtain a relationship between it and Δn , the carrier induced index change in the active layer. In theory, the absolute frequency f , is governed by an integer mode number, m , the velocity of light, c , the effective index of the waveguide, n_e , and the cavity length L . If the active layer index is increased by Δn then the resonant frequency will become [34]

$$f = cm / \left[2L \left(n_e + \frac{\delta n_e}{\delta n} \frac{\Delta n_e}{n_e} \right) \right] \quad (7)$$

$\delta n_e / \delta n$ serves to dilute the effect of the active layer index change and is commonly made equal to the confinement factor, Γ [17].

The TLLM in Reference 10 uses a non-dispersive transmission line to model the cavity. To obtain the correct mode spacing, the phase velocity in the cavity (c/n_e) was approximated to the group velocity (c/\bar{n}_e). A modified mode number, which will now be called \bar{m} , was then used to set the model's resonant frequency to within one half of one mode of the absolute frequency. This inaccuracy is unimportant as it is the relative position of mode and gain peak which determines the spectrum of the laser [15]. If the model's length is increased by l , its resonant frequency will be given by

$$f = \bar{m}c / [2\bar{n}_e(L + l)] \quad (8)$$

Equating eqns. 7 and 8, and when l and Δn are zero gives

$$\bar{m} = m\bar{n}_e/n_e \quad (9)$$

This can be substituted into eqns. 7 and 8 to give the required relationship between the model's change in

length, and the change in effective index

$$l = \frac{\delta n_e}{\delta n} \frac{\Delta n}{\bar{n}_e} L = \Gamma \frac{\Delta n}{\bar{n}_e} \quad (10)$$

It is interesting to investigate the change in mode spacing in a similar manner. The theoretical mode spacing, f' , is given by

$$f' = c/[2L(\bar{n}_e + \Delta\bar{n}_e)] \quad (11)$$

where $\Delta\bar{n}_e$ is the induced change in group index.

The model mode spacing, f'_m is given by eqn. 8 with \bar{m} unity

$$f'_m = c/[2\bar{n}_e(L + l)] \quad (12)$$

With $\Delta\bar{n}_e$, and l set to zero, the model is in exact agreement with theory, as expected. The model is also approximately correct if the change in group effective index, $\Delta\bar{n}_e$ approximates to the change in effective index, Δn_e .

The change in active layer index is assumed to be linearly dependent upon carrier concentration, i.e.

$$\Delta n = \frac{\delta n}{\delta N} (N - N_{th}) \quad (13)$$

where

N is the average carrier concentration in the cavity
 N_{th} is the threshold carrier concentration
 $\delta n/\delta N$ is the rate of change of n with N

Strictly, the average index along the cavity should be calculated by invoking the above equation at each model section along the cavity. However, for small index changes the above approximation is valid, and is also consistent with other models which neglect longitudinal effects [30, 31]. It shall therefore be used in this paper.

The factor $\delta n/\delta N$ can be obtained directly from experimental results or indirectly from the gain constant, g , the confinement factor, the resonant frequency, and the linewidth enhancement factor, α [17]

$$\frac{\delta n}{\delta N} = -\frac{\alpha c}{4\pi f} \frac{\delta g}{\delta N} \quad (14)$$

The linewidth enhancement factor used in the following analysis is 5.6 [34], which in general agrees with values given in Reference 17 for 1.55 μm devices. This will be used to obtain an analytical result for the linewidth of the laser.

The consequences of undersampling, i.e. at less than the Nyquist sampling frequency, must be considered. Undersampling drastically reduces computing time, by increasing the iteration timestep, ΔT , and reducing the number of model sections, s . Two effects are: (a) decrease in the model's bandwidth (b) a reduction in the accuracy in the Taylor series expansion of the gain curve term [10].

An added effect, for the SA model, is to reduce the accuracy of the longitudinal mode positions. This is because the stub models an almost constant impedance, and its own impedance ranges from infinity to zero across the model's bandwidth. As the impedances are matched at the resonance frequency, f , then the important modes close to this are accurately placed. However, at the band edges, the mode spacing becomes compressed; as shown in Fig. 2, in which the longitudinal mode positions are plotted against the added cavity length at each facet, for a 25 section model. This also shows the modes around the resonant frequency, the frequency of which has a linear dependence upon cavity length, and shifts by

two modes when the cavity is extended by one wavelength, as expected.

4 A 1550 nm laser example

A 1550 nm double-heterojunction semiconductor laser has been chosen to demonstrate the method, as this is the

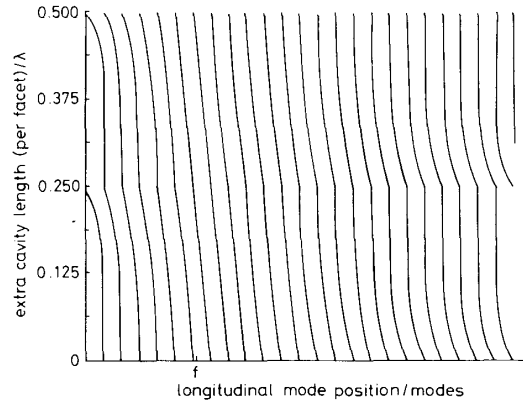


Fig. 2 Longitudinal mode shift with extra length added at each facet, $f = 1$ laser resonance frequency

optimum wavelength device for long haul systems using silica fibres [3]. It is in these systems that bandwidth is likely to be limited by fibre dispersion. Ideally, the laser should be single moded, however this is unlikely to be the case without the use of external cavities [35], coupled cavities [36], or a distributed feedback grating [37]. In this example, a multi-mode device with a 190 μm cavity is modelled.

The material parameters are taken from a paper by Westbrook [34] and have been found from a InGaAsP ridge-waveguide structure. The modelled device is a stripe geometry, built-in waveguide structure that is assumed to have the same material parameters as the above device. Westbrook specifies the material gain thus

$$g = a_1(N - N_0) - a_2[hv - (E_0 + a_3(N - N_0))]^2$$

where

g is the material gain per unit length
 a_1 is dg/dN at the gain curve peak ($2.7 \times 10^{-16} \text{ cm}^2$)
 N_0 is the transparency carrier density ($9 \times 10^{17} \text{ cm}^{-3}$)
 a_2 is the parabola width parameter ($4 \times 10^5 \text{ eV}^{-2} \text{ cm}^{-1}$)
 a_3 is dE_0/dN the gain peak position carrier dependence ($1.4 \times 10^{-20} \text{ cm}^3 \text{ eV}$)

This equation may be rearranged into the parabolic form used by Buus [38]

$$g = a_1(N - N_0) \{1 - a_2[hv - E_0 - a_3(N - N_0)]^2/[a_1(N - N_0)]\}$$

This is easily equated to the Lorentzian form used in the TLLM, by matching the gain at the gain peak, and at one mode away from it. This process yields the Q of the gain curve that is carrier dependent

$$Q = \sqrt{(\delta/2)f/\Delta f}$$

where δ is Buus' parameter given by

$$\delta = a_2(h\Delta f)^2/[a_1(N - N_0)]$$

In this analysis, the Q -factor is fixed at its threshold value. Also, the gain peak position carrier dependence is

set to zero, as it is the linewidth of the individual modes that is under investigation, and not the power distribution amongst the modes.

The cavity dimensions and reflectivities are typical for single-transverse mode devices, and are detailed in Table 1. The model parameters have been calculated with the equations given in [10].

Table 1: Modelled laser parameters

| Symbol | Parameter | Value | Units |
|-------------|-------------------------------|--------------------------|------------------|
| λ_0 | Free space wavelength | 1.5 | μm |
| L | Cavity length | 190 | μm |
| d | Active region depth | 0.15 | μm |
| w | Active region width | 5.00 | μm |
| \bar{n}_e | Group index | 3.7 | |
| n_e | Effective index | 3.4 | |
| R | Facet reflectivities | 0.3 | |
| Q | Gain curve Q -factor | 22 | |
| B | dg/dN | 2.7×10^{-16} | cm^2 |
| Γ | Confinement factor | 0.3 | |
| N | Transparency Carrier Density | 9.0×10^{17} | cm^{-3} |
| a | Linewidth enhancement factor | 5.6 | |
| a_{sc} | Internal attenuation factor | 15 | cm^{-1} |
| τ_s | Carrier lifetime | 1.7×10^{-9} | s |
| β | Spontaneous emission coupling | 1.0×10^{-4} | |
| ΔT | Model timestep | 9.3733×10^{-14} | s |
| s | Number of sections | 25 | |
| b | Band-number | 18 | |

A choice of 25 sections along the cavity gives a modelled bandwidth of 25 longitudinal modes and a gain curve accuracy of 98.5%. This is a compromise between modelling speed and accuracy. The former being approximately 25 minutes for 1 ns of laser time on a Whitechapel MG1 Workstation, which is larger than that predicted in [10], because of the inclusion of a carrier diffusion model based on Reference 39 into the TLLM. The latter may be judged from Figs. 2 and 3, which give an estimate of

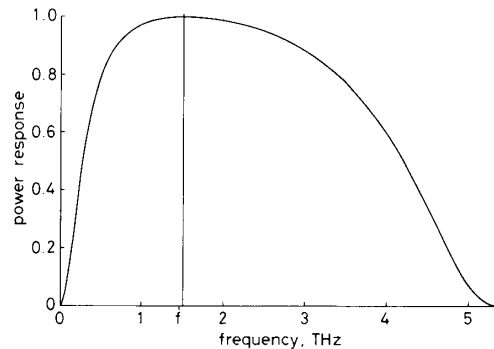


Fig. 3 Gain curve filter response over modelled bandwidth

mode position accuracy and gain curve accuracy, respectively. The gain curve is accurate in the important region around the laser resonance, but is truncated because of the model's small bandwidth. The extra cavity length, required to model the refractive index variation, has been divided between the two facets. The length per facet has been set to one quarter of a wavelength at the threshold carrier density.

The spontaneous emission coupling factor to the dominant mode, β , has been calculated as approximately 0.0001 [40]. This has been matched to the form used in the TLLM by matching the peak to mean power ratio of the TLLM to that of a multi-mode numerical solution of the rate equations. This gives 0.03 as the value of β used in the TLLM. A more fundamental method of represent-

ing spontaneous emission in the model will be introduced in a future publication.

The model was tested using a step in injection current of various values applied at zero time, with the initial carrier density set to $1.5 \times 10^{18} \text{ cm}^{-3}$, slightly above the threshold value. This transient will cause ringing of the laser power output, observed as a series of pulses. It is assumed that the injection current would be terminated soon after the first pulse, to achieve high transmission rates, although it may be of advantage to lengthen the pulse by modulation pulse shaping [40] when low bit rates are used. However, a detailed analysis and optimisation of pulse shape is beyond the scope of this introductory paper, and hence it is the first of a series of pulses that will be analysed. Thus, for each run, the iterations were continued until the first minimum after the first optical pulse. Fig. 4 shows the pulse shape for modulation currents of 20 mA to 150 mA giving pulse widths of

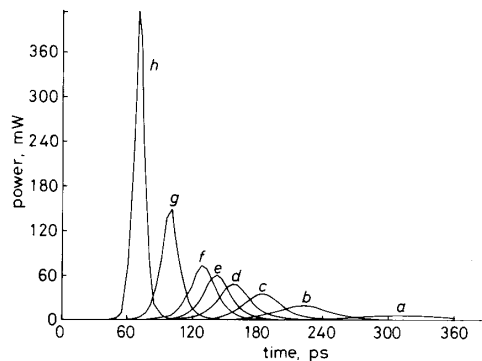


Fig. 4 Optical output pulse for various values of current
a 20 mA; b 25 mA; c 30 mA; d 35 mA; e 40 mA; f 45 mA; g 70 mA; h 150 mA

10 to 95 ps. As expected, increasing the injection current decreases the delay time and the pulse width whilst the peak power output is increased.

Fourier transforms of the modelled interval were then taken to obtain the spectra of the pulses, the resolution of these spectra being limited by the period over which they were taken. Fig. 5(a-d) shows selected spectra, all of

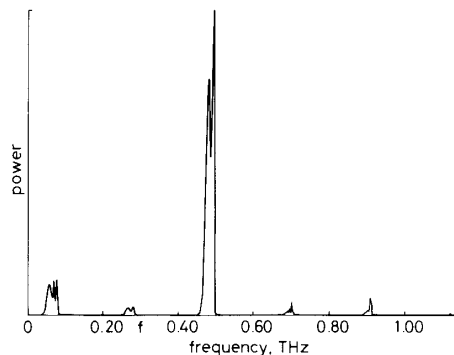


Fig. 5a Transform of pulse a

which show the classical 'rabbit-ear' lineshape, of each longitudinal mode. A simple check of the maximum frequency deviation against the difference between maximum and minimum carrier densities during the optical pulse eqn. 7 shows that the model is quantitatively correct. For a qualitative assessment experimental results presented by: van der Ziel [22] and Hakki [23]

for GaAs devices, and Lin, Lee & Burrus [41] and Dutta *et al.* [24, 25] for InGaAsP devices are used. The frequency chirp in References 23 and 22 is a result of self

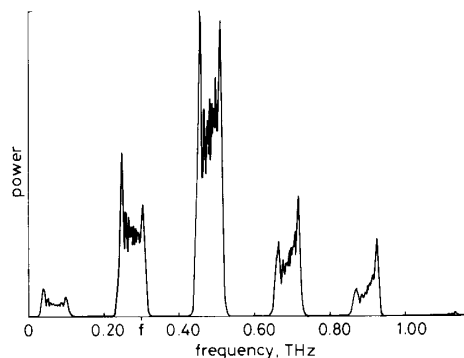


Fig. 5b Transform of pulse c

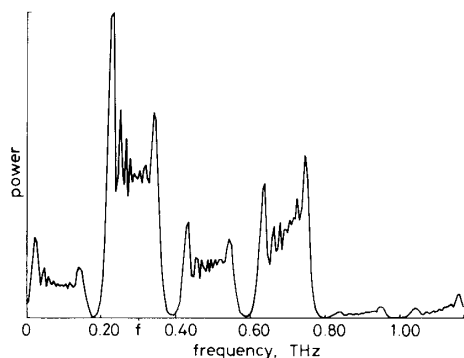


Fig. 5c Transform of pulse g

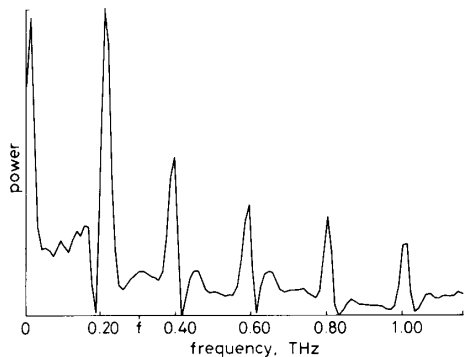


Fig. 5d Transform of pulse h

induced modulation (self-pulsation). In [24, 25] the chirp is caused by a sine-wave modulation of the injection current, whereas in Reference 41 picosecond pulse modulation is used.

The multimode spectra of References 22 and 23 show good agreement with those presented herein. The frequency chirp of each mode is essentially of equal magnitude [22]. The ear lengths of the modes around the gain-peak are nearly equal, whereas at the longer wavelength modes the long-wavelength ears are preferred, and conversely, the short wavelength ears are dominant at shorter wavelengths [23]. This effect is attributed to the gain curve position dependence on carrier density, in the above paper. However, as this dependence is not modelled, then some other mechanism must be responsible.

One possible explanation could be the influence of the gain curve filters' phase shift or amplitude response on the resonance frequency. However, both these effects tend to reinforce the ear closest to the laser's resonance. Another theory, providing the required answer, is that the farthest away ear collects more spontaneous emission power over a larger frequency range, as the Q of the cavity mode is smaller when less gain is present.

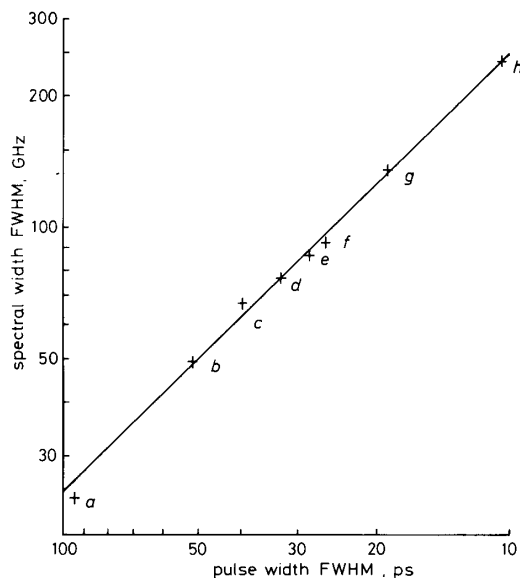


Fig. 6 Spectral width against pulse width for the drive currents given in Fig. 4

The solid line is the analytical result for $\alpha = 5.6$

The sine-wave modulation results for a series of peak to peak currents [24, 25] show the expected trend of high chirp for large modulation. However, because of the integrating effect of the measurement system, the fine random-noise induced detail on the rabbit's forehead is missing. Reference 24 also includes results for a GRIN-rod external cavity laser, which could be modelled with the TLLM by simulating the external cavity with a series of passive transmission lines. This is an obvious path to follow in the development of the model. Results for very short optical pulses (40 ps) from both long and short cavity lasers are given in Reference 41. Unfortunately, the resolution of the spectrometer is too poor to resolve the individual ears from the forehead, but it is good enough to show the asymmetry of the modes. The sense of the shift, i.e. blue to red during the pulse peak, agrees with the TLLM, and justifies the sign of α .

It is interesting to compare the results with the analytical formula (eqn. 1) obtained in References 7, 8, 21 for a Gaussian pulse. For this purpose, the linewidth of an individual mode (FWHM) is plotted against the optical pulsewidth (FWHM) in Fig. 5. Logarithmic scales are used so that lines of constant time-bandwidth product (TBP) may be plotted. The results show that the values of TBP are close to that predicted by (1), lying slightly below theory for low currents. This appears a useful result, as the analytical formula could be used in the calculation of dispersion in fibres but, is in fact worthless as the formula gives no indication of where the power lies within the mode spectrum.

5 Conclusions

Experimental and theoretical results from other workers show that laser chirp is a significant contribution to the linewidth of near single-mode lasers, and therefore a good model of this is required when the dispersion in long-haul fibre systems is to be calculated. A transmission line laser model including chirp has been developed to fulfill this requirement, which is reasonably fast and has suitable time-domain interfaces to both fibre and drive circuit models. Various methods of including chirping to the original TLLM were considered before the stub-attenuator model was chosen. This models index variation by altering the effective length of the cavity by the use of transmission line stubs and attenuators to replace the end-facets. The stub and attenuator are then represented by a simple scattering matrix. The modal positions have been shown to be accurate near the laser's resonance frequency, even when a reduced modelling bandwidth is used to minimise computing time. A model of a 1550 nm device under picosecond pulse modulation gives good results comparable with both experimental and analytical data, and shows the classic rabbit ear spectrum. The model may be particularly useful for calculating optimum injection current pulse shape for low linewidth. As the model is a close analogue to the real device it may be easily modified to cover external cavity and multi-contact lasers. Other future applications may be bistable laser amplifiers, and cleaved coupled-cavity devices.

References

- MARCUSE, D.: 'Pulse distortion in single-mode fibres', *Appl. Opt.*, 1980, **19**, pp. 1653-1660
- MARCUSE, D.: 'Pulse distortion in single-mode fibres. Part 2', *Appl. Opt.*, 1981, **20**, pp. 2969-2974
- BOTEZ, D.: 'Single-mode lasers for optical communications', *IEE Proc. Pt. 1*, 1982, **129(I)**, pp. 237-251
- MARCUSE, D.: 'Pulse distortion in single-mode fibres. 3: Chirped pulses', *Appl. Opt.*, 1981, **20**, pp. 3573-3579
- IWASHITA, K., NAKAGAWA, K., NAKANO, Y., and SUZUKI, Y.: 'Chirp pulse transmission through a single-mode fibre', *Electron. Letts.*, 1982, **18**, pp. 873-874
- LINKE, R.A.: 'Transient chirping in single-frequency lasers: light-wave systems consequences', *Electron. Letts.*, 1984, **20**, pp. 472-474
- BUUS, J.: 'Propagation of chirped semiconductor laser pulses in monomode fibres', *Appl. Opt.*, 1985, **24**, pp. 4196-4198
- KOYAMA, F., and SUEMATSU, Y.: 'Analysis of dynamic spectral width of dynamic single-mode (DSM) lasers and related transmission bandwidth of single-mode fibres', *IEEE J. Quantum Electron.*, 1985, **QE-21**, pp. 292-297
- BUUS, J.: 'Principles of semiconductor laser modelling', *IEE Proc. J.*, 1985, **132**, pp. 42-51
- LOWERY, A.J.: 'New dynamic semiconductor laser model based on the transmission line modelling method', *IEE Proc. J.*, 1987, **134**, pp. 281-290
- JOHNS, P.B., and BEURLE, R.L.: 'Numerical solution of 2-dimensional scattering problems using a transmission line matrix', *IEE Proc.*, 1971, **118**, pp. 1203-1208
- JOHNS, P.B.: 'The solution of inhomogeneous waveguide problems using a transmission-line matrix', *IEEE Trans. Mic. Theory & Techniques*, 1974, **MTT-22**, pp. 209-215
- PETERMANN, K.: 'Theoretical analysis of spectral modulation behaviour of semiconductor injection lasers', *Opt. & Quant. Electron.*, 1978, **10**, pp. 233-242
- OTSUKA, K., and TARUCHA, S.: 'Theoretical studies on injection locking and injection induced modulation of laser diodes', *IEEE J. Quantum Electron.*, 1981, **QE-17**, pp. 1515-1521
- ADAMS, M.J., and OSINSKI, M.: 'Longitudinal mode competition in semiconductor lasers: rate equations revisited', *IEE Proc. Pt. 1*, 1982, **129(I)**, pp. 271-274
- HENRY, C.H.: 'Theory of the linewidth of semiconductor lasers', *IEEE J. Quantum Electron.*, 1982, **QE-18**, pp. 259-264
- OSINSKI, M., and BUUS, J.: 'Linewidth broadening factor in semiconductor lasers — an overview', *IEEE J. Quantum Electron.*, 1987, **QE-23**, pp. 9-29
- HENNING, I.D., and COLLINS, J.V.: 'Measurements of the semiconductor linewidth broadening factor', *Electron. Letts.*, 1983, **19**, pp. 927-929
- OTSUKA, K., and KOBAYASHI, S.: 'Optical bistability and non-linear resonance in a resonant-type semiconductor laser amplifier', *Electron. Letts.*, 1983, **19**, pp. 262-263
- LIN, C., EISENSTEIN, G., BURRUS, C.A., and TUCKER, R.S.: 'Temporal and spectral characteristics of single-longitudinal-mode short-coupled cavity (SCC) InGaAsP Lasers under multigigahertz direct modulation', *Electron. Letts.*, 1984, **20**, pp. 842-844
- KOCH, T.L., and BOWERS, J.E.: 'Nature of wavelength chirping in directly modulated semiconductor lasers', *Electron. Letts.*, 1984, **20**, pp. 1038-1039
- VAN DER ZIEL, J.P.: 'Spectral broadening of pulsating Al(x)Ga(1-x)As double heterostructure lasers', *IEEE J. Quantum Electron.*, 1979, **QE-15**, pp. 1277-1281
- HAKKI, B.W.: 'Optical and microwave instabilities in injection lasers', *J. Appl. Phys.*, 1980, **51**, pp. 68-73
- OLSSON, N.A., DUTTA, N.K., and LIU, K.-Y.: 'dynamic linewidth of amplitude modulated single-longitudinal-mode semiconductor lasers operating at 1.5 μm wavelength', *Electron. Letts.*, 1984, **20**, pp. 121-122
- DUTTA, N.K., OLSSON, N.A., KOSZI, L.A., BESOMI, P., WILSON, R.B., and NELSON, R.J.: 'Frequency chirp under current modulation in InGaAsP injection lasers', *J. Appl. Phys.*, 1984, **56**, pp. 2167-2169
- CARROLL, J.E., WHITE, I.H., and GALLAGHER, D.F.G.: 'Dependence of chirp in injection lasers on temporal optical pulse shape', *IEE Proc. J., Optoelectron.*, 1986, **133**, pp. 279-282
- LINKE, R.A.: 'Modulation induced transient chirping in single frequency lasers', *IEEE J. Quantum Electron.*, 1985, **QE-21**, pp. 593-597
- TSUSHIMA, H., and SUEMATSU, Y.: 'Large-signal analysis of dynamic wavelength shift and carrier-density-variation in directly modulated dynamic single-mode lasers', *Trans. IECE Japan.*, 1984, **E-67**, pp. 480-487
- ANDERSSON, P., and ANDERSSON, T.: 'Chirp in picosecond pulses from diode lasers: dependence on the modulation conditions and the linewidth enhancement factor', *IEEE J. Lightwave Tech.*, 1986, **LT-4**, pp. 795-798
- ABDULA, R.M., and SALEH, B.E.A.: 'Dynamic spectra of pulsed laser diodes and propagation in single-mode fibres', *IEEE J. Quantum Electron.*, 1986, **QE-22**, pp. 2123-2130
- OSINSKI, M., and ADAMS, M.J.: 'Transient time-averaged spectra of rapidly-modulated semiconductor lasers', *IEE Proc. J.*, 1985, **132**, pp. 34-37
- OSINSKI, M., and ADAMS, M.J.: 'Picosecond pulse analysis of gain-switched 1.55 μm InGaAsP lasers', *IEEE J. Quantum Electron.*, 1985, **QE-21**, pp. 1929-1936
- BICKERS, L., and WESTBROOK, L.D.: 'Reduction of transient laser chirp in 1.5 μm DFB lasers by shaping the modulation pulse', *IEE Proc. J.*, 1986, **133**, pp. 155-162
- WESTBROOK, L.D.: 'Measurements of dg/dN and dn/dN and their dependence on photon energy in $\lambda = 1.5 \mu\text{m}$ InGaAs laser diodes', *IEE Proc. J.*, 1986, **133**, pp. 135-142
- COLDREN, L.A., and KOCH, T.L.: 'External-cavity laser design', *IEEE J. Lightwave Tech.*, 1984 **LT-2**, pp. 1045-1051
- TSANG, W.T., OLSSON, N.A., and LOGAN, R.A.: 'Stable single-longitudinal-mode operation under high-speed direct modulation in cleaved-coupled-cavity GaInAsP semiconductor lasers', *Electron. Letts.*, 1983, **19**, pp. 488-490
- KAWANISHI, H., SUEMATSU, Y., UTAKA, K., ITAYA, Y., and ARIA, S.: 'Ga(x)In(1-x)As(y)P(1-y)/InP injection laser partially loaded with first-order distributed Bragg reflector', *IEEE J. Quantum Electron.*, 1979, **QE-15**, pp. 701-706
- BUUS, J.: 'Simple theory for the spectral properties of semiconductor lasers with reduced reflectivity', *IEE Proc. J.*, 1986, **133**, pp. 121-123
- JOHNS, P.B.: 'A simple, explicit, and unconditionally stable numerical routine for the solution of the diffusion equation', *Journal for Numerical Methods in Engineering*, 1977, **11**, pp. 1307-1328
- OLSHANSKY, R., and FYE, D.: 'Reduction of dynamic linewidth in single-frequency semiconductor lasers', *Electron. Letts.*, 1984, **20**, pp. 928-929
- LIN, C., LEE, T.P., and BURRUS, C.A.: 'Picosecond frequency chirping and dynamic line broadening in InGaAsP injection lasers under fast excitation', *Appl. Phys. Lett.*, **42**, pp. 141-143